Determination of the Harmonic Losses in an Induction Motor Fed by an Inverter

Bilal Abdullah Nasir
Department of Electrical Techniques
Northern Technical University
Mosul, Iraq
bilalalnasir@ntu.edu.iq

Received: 24 April 2022 | Revised: 16 May 2022 | Accepted: 19 May 2022

Abstract-The advancement, development, improvement, and increased use of power electronic converters led to the efficient speed control of electrical drives. The most famous three-phase induction motor-related control to Pulse-Width Modulation (PWM) technique is used to operate multilevel inverters such as variable-frequency or six-step Voltage Source Inverter (VSI). Switching devices of the inverter are used in the drive systems and act as the main source of harmonics. When the induction motor is fed from the PWM inverter, it will be supplied by low order (5th, 7th, 11th) time harmonic voltage. The motor performance is affected by the presence of these time harmonic components because the additional losses generated in the motor defect its performance, generate pulsating torque, and reduce efficiency. In this work, the analysis of a dynamic model of an induction motor in transient and steady-state operation is developed, considering the effect of time-harmonic voltages generated by the inverter, skin effect, skew effect, temperature rise effect, iron core loss, stray load loss, and magnetic saturation on the motor performance. The performance of the motor is studied by the time-harmonic equivalent circuit and by the fundamental equivalent circuit. The motor performance in terms of efficiency and power factor is compared with the experimental results for both sinusoidal and VSI motor feeds in order to validate the model accuracy.

Keywords-dynamic modeling; additional losses; 3-phase bridge inverter; 3-phase diode rectifier; harmonic equivalent circuit; switching functions

I. INTRODUCTION

It has been observed that the electrical machine losses increase if the supply voltage has harmonics. This gained attention at the early '70s, as the machines were supplied with static six-step inverters. The additional Ohmic losses were produced in the machine windings due to the flowing of harmonic currents. The Ohmic losses in the rotor windings of the induction machines can increase considerably due to the skin effect. There is also an increase in the machine iron losses due to the flowing of harmonic currents [1-5]. At low harmonic frequency (< 2.5kHz), the harmonic losses are also increased with the machine load due to the slight reduction of the machine inductances caused by the saturation effect [6-7]. Measuring the harmonic losses in electrical machines is a very complex task, and its determination by subtracting the output power from the input power is very sensitive to errors of measurement [8]. At the beginning of this century, the calculation of harmonic losses was extended by numerical methods with computer analysis based on the Finite Element Method (FEM) [9-11]. In numerical methods, the computational process is a heavy burden and the complete structure of the machine has to be known [12]. The early adopted six-step inverters showed a defect in machine performance due to the pulsating torques and increasing harmonic losses [13-14]. In modern semiconducting techniques, the switching frequency and modulation index of PWM variable speed drives can be allowed to be further increased and eliminate all harmonics below the switching frequency. Although this technique can increase the machine performance and reduce noise emissions, the machine harmonic losses cannot be reduced considerably by increasing the switching frequency above 10kHz [15-24]. To model the harmonic losses of the induction machines with different power ratings, a complete equivalent circuit including all harmonic loss components was first presented in [5]. In this circuit, the resistances are connected in parallel to the leakage inductances accounting for the harmonic stray load losses in the machine windings. The harmonic losses due to the skew-effect and skin-effect are not included in this equivalent circuit model. All the equivalent circuit impedances must be frequency-dependent to take effect on the skin [25-28].

Variable speed drives are commonly used in many industrial applications. To supply the motor with variable frequency, the induction motor is fed from the six-step uncontrolled rectifier and the rectifier output is connected to the six-step Voltage Source Inverter (VSI). Two capacitors are connected across the rectifier output to remove the ripple. Due to the motor being fed from the switching inverter, the dynamic model developed to study the motor performance must be valid for any voltage and current waveform. A complete dynamic model is required for harmonics analysis. The model must include the main parameters of the machine for transient and steady-state operation. In this paper, an accurate dynamic model of the induction motor fed from a six-step VSI is presented using the switching functions for inverter modeling and the D-Q axes synchronously rotating reference frame

Corresponding author: Bilal Abdullah Nasir

model for induction motor modeling. In this comprehensive modeling, the harmonics, as additional losses, are calculated and analyzed easily. The accuracy of the model has been verified through Matlab simulations and the harmonic equivalent circuit of the machine, which is presented in this work as a powerful tool for motor performance calculation.

II. MODELING OF THE INDUCTION MOTOR

An accurate estimation parameter of the induction motor-equivalent circuit is required to implement these parameters for high-performance determination. The stator and rotor winding temperatures can be determined according to the IEEE standard 112-B by measuring the stator no-load and load currents, and the rotor current is determined at different load conditions. The skin effect on the stator parameters can be determined from the stator geometry. The iron core resistances are determined from the no-load test considering the effect of slip and core temperature. The magnetizing reactance is calculated from the no-load test at different supply voltages and rated frequencies to consider the saturation effect. The stator and rotor winding resistances R_s and $\acute{R}_r$ depend on temperature variation and skin effect. The stator and rotor leakage reactances $X_{\ell s}$ and $\acute{X}_{\ell r}$ depend on skin effect and saturation. The magnetizing inductance X_m depends on the magnetic saturation. The iron core resistance R_{ic} depends on motor slip and iron core temperature.

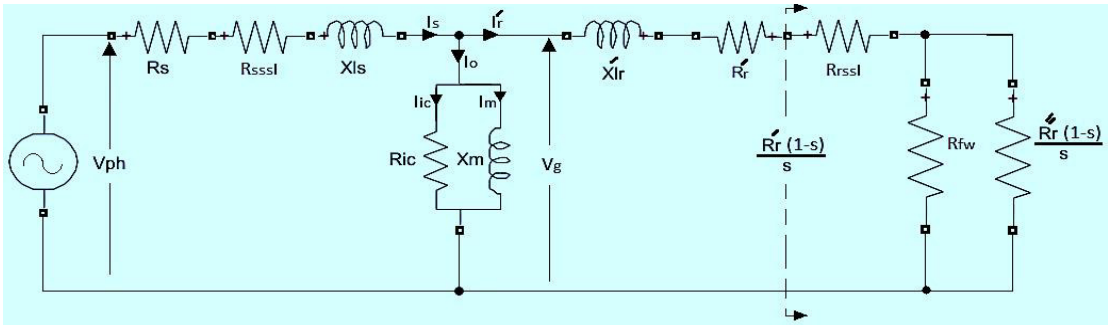

Fig. 1. The proposed fundamental circuit of induction motor.

The proposed equivalent circuit in Figure 1 contains the additional resistances $R_{sss\ell}$ and $R_{rss\ell}$ that model the stray losses in the stator and rotor circuits. The stray losses depend on the voltage drops due to the leakage reactance, the iron core resistances, and stator and rotor resistance. Also, the proposed equivalent circuit can deal with the effect of rotor skewing on the parameters of the rotor circuit. The iron core resistance is varied with the temperature and air-gap voltage and is calculated from the no-load test of the motor as [25]:

$$R_{ic} = V_g^2 \,/\, [K_T * (P_{n\ell} - I_o^2 * R_s)] \quad (1)$$

$$V_g = X_m * I_m = X_m * I_o * \sin(\phi_o) \quad (2)$$

$$I_m = \left[\frac{Q_{n\ell} - I_o^2 * X_{\ell s}}{X_m}\right]^{\frac{1}{2}} \quad (3)$$

where V_g is the magnetizing voltage per phase and is calculated in terms of magnetizing reactance X_m, magnetizing current I_m, no-load current I_o, and no-load sine of power factor angle $\sin\varphi_o$. The iron core resistance was obtained in terms of air-gap voltage from the no-load test and curve-fitting technique [25]. K_T= (1-D) is the temperature coefficient of the iron core loss, and D is the iron core power loss varying rate per ^oC determined as [25]:

$$D = \left[P_{ic\,(To)} - P_{ic\,(T)}\right] / P_{ic\,(To)} \quad (4)$$

where $P_{ic\,(To)}$ and $P_{ic\,(T)}$ represent the iron core power losses at ambient temperature and at any temperature. These iron core power losses are measured from the no-load test. $P_{n\ell}$ is the active no-load power loss per phase, R_{so} is the stator resistance per phase at ambient temperature, $Q_{n\ell}$ is the reactive no-load power loss per phase, and $X_{\ell s}$ is the stator leakage reactance per phase. The rotor load resistance $\acute{R}_r(1-s)/s$ is derived in terms of rotor phase resistance $\acute{R}_r$ and rotor series stray loss resistance $R_{rss\ell}$ as:

$$\acute{R}_r(1-s)/s \;\; = 1/\left[1/\left\{\frac{\acute{R}_r(1-s)}{s} - R_{rss\ell}\right\} - 1/R_{f\omega}\right] \quad (5)$$

where $R_{f\omega}$ is the mechanical loss resistance. The nonlinearity of the machine iron core and mechanical resistances due to the saturation of the magnetic core is considered by the dynamic model to improve the accuracy of simulation results. The resistances R_{ic} and $R_{f\omega}$ are determined practically from the no-load test at zero slip to be modeled by polynomial-curve fitting as:

$$R_{ic} = -0.0001985 * V_g^3 + 0.111 * V_g^2 - 23.11 * V_g + 840 \quad (6)$$

$$R_{fw} = -6.167 * V_g^4 + 0.00419 * V_g^3 - 1.074 * V_g^2 + 127.4 * V_g + 560 \quad (7)$$

The resistance of the iron core R_{ic} can be referred to on the stator and rotor circuits as a voltage drop to keep the dynamic 4th order model fixed while the effect of the iron core loss in the dynamic model of Figure 2 is considered. The reflecting resistances on the stator circuit R_{ssic} and on the rotor circuit R_{rsic} are calculated as [26]:

$$R_{ssic} = (R_{ic} * \omega_s * L_M) \,/\, [R_{ic}^2 + (\omega_s + L_M)^2] \quad (8)$$

$$R_{rsic} = s * R_{ssic} \quad (9)$$

where s is the motor slip and L_M is the magnetizing inductance per phase obtained from the no-load test as:

$$L_M = X_m / \omega_s \quad (10)$$

where $\omega_s = (2 * \pi * f)$ is the angular frequency in rad/s.

The modified magnetizing inductance L_m of the dynamic model (Figure 2) is calculated as:

$$L_m = L_M * R_{ic}^2 / [R_{ic}^2 + (\omega_s * L_M)^2] \quad (11)$$

The stray load loss resistances vary with the variation of stator and rotor resistances due to the temperature variation. These resistances are derived and introduced in the dynamic model as series resistances in the stator and rotor circuits [27]:

$$R_{sss\ell} = (\omega_s * L_{\ell s})^2 * R_s / [R_s^2 + (\omega_s * L_{\ell s})^2] \quad (12)$$

$$R_{rss\ell} = S^2 * (\omega_s * L'_{\ell r})^2 / R'_r \quad (13)$$

where $R_{sss\ell}$ and $R_{rss\ell}$ are the series stator and rotor winding stray-load loss resistances respectively, S is the motor slip, and $L_{\ell r}$ is the rotor leakage inductance per phase.

All induction motors and generators operate in the saturation region and their characteristics are non-linear. The variation of magnetizing reactance X_m is the main factor in producing the magnetizing voltage V_g, which is the main factor that produces the iron-core losses, rotor current, mechanical losses, and output power. The saturation reduces V_g and tends to increase. The saturation effect is taken by the relation $X_m = f(I_m)$. This function is obtained practically from the no-load test by varying the supply voltage from 125% to 25% of the rated value. Then the measurements of X_m and I_m can be interpolated by the curve fitting technique.

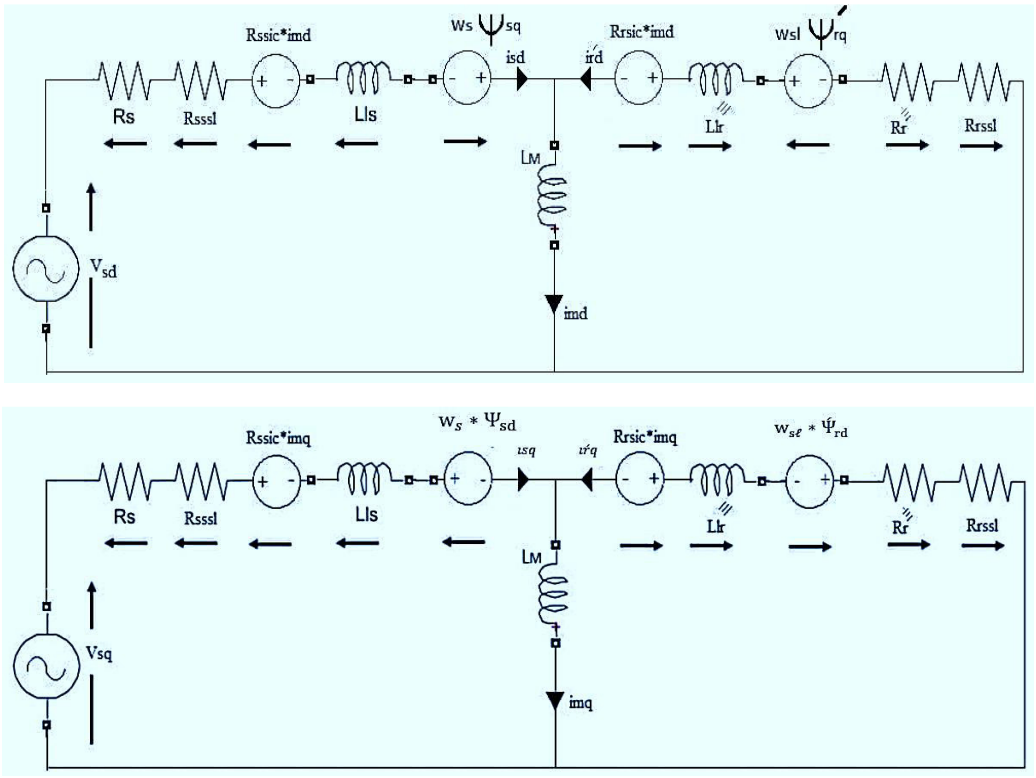

Fig. 2. (a) D-axis and (b) Q-axis equivalent circuit models of the induction motor in the synchronously rotating frame.

The rotor phase leakage reactance $\acute{X}_{\ell r}$ is corrected by the skew factor K_{sq} [25]:

$$\acute{X}_{\ell r} = \frac{X_m}{K_{sq}^2}\left(1 - K_{sq}^2\right) + \frac{\acute{X}_{\ell r}}{K_{sq}^2} \quad (14)$$

$$K_{sq} = sin\left(\frac{\pi * P_p}{Q_r}\right) / \left(\pi * P_p / Q_r\right) \quad (15)$$

where P_p is the machine magnetic pole-pair, and Q_r is the number of rotor slots (bars).

The rotor phase resistance is corrected by the skew factor as:

$$\acute{R}_r = \acute{R}_r / K_{sq}^2 \quad (16)$$

The rotor phase resistance and leakage reactance are corrected by the skin effect as [25]:

$$\acute{\acute{R}}_r = \acute{\acute{R}}_r * \left[\, 0.5 + 0.5 * \sqrt{S_r / S_m}\, \right] \quad (17)$$

$$\acute{\acute{X}}_{\ell r} = \acute{\acute{X}}_{\ell r} * \left[\, 0.4 + 0.6 * \sqrt{S_m / S_r}\, \right] \quad (18)$$

where S_r is the rated machine slip and S_m is the machine slip at maximum torque which can be given as [27]:

$$S_m = (\acute{R}_r + R_{rss\ell}) / \left[(R_s + R_{sss\ell})^2 + (X_{\ell s} + \acute{X}_{\ell r})^2\right]^{½} \quad (19)$$

Also, the machine slip can be corrected due to the temperature effect as [25]:

$$\acute{S}_{r,m} = S_{r,m} * (T_r + K_a) \,/\, (T_{ref} + K_a) \quad (20)$$

where T_r is the rotor bar temperature at any load, T_{ref} is the temperature of insulation class level, which can be obtained from the insulation class table, and K_a is a constant equal to 225 for aluminum rotor bar type.

The dynamic electrical equations of the induction motor are derived from the proposed equivalent circuit in Figure 2 as:

$$v_{sd} = (R_s + R_{sss\ell} + R_{ssic})\, i_{sd} + R_{ssic} * \acute{\imath}_{rd} - \omega_s * L_m * \acute{\imath}_{rq} \quad (21)$$

$$v_{sq} = \omega_s * (L_{\ell s} + L_m) * i_{sd} + \omega_s * L_m * \acute{\imath}_{rd} \quad (22)$$

$$o = R_{rsic} * i_{sd} + \left(\acute{\acute{R}}_r + R_{rss\ell} + R_{rsic}\right) * \acute{\imath}_{rd} + \omega_{s\ell} * \left(\acute{\acute{L}}_{\ell r} + L_m\right) \acute{\imath}_{rq} \quad (23)$$

$$o = \omega_{s\ell} * L_m * i_{sd} + \omega_{s\ell} * \left(\acute{\acute{L}}_{\ell r} + L_m\right) * \acute{\imath}_{rd} + \left(\acute{\acute{R}}_r + R_{rss\ell} + R_{rsic}\right) * \acute{\imath}_{rq} \quad (24)$$

where $\omega_{s\ell} = \omega_s - \omega_r = s * \omega_s$ is the slip speed in rad/s, $\omega_r = P_p * \omega_m$ is the electrical angular speed of the motor in rad/s, and ψ_{sd} , ψ_{sq} , $\acute{\psi}_{rd}$ and $\acute{\psi}_{rq}$ are the stator and rotor flux linkages in the D-Q axes of Figure 2 respectively, defined as :

$$\psi_{sd} = L_{\ell s} * i_{sd} + L_m * i_{md} \quad (25)$$

$$\psi_{sq} = L_{\ell s} * i_{sq} + L_m * i_{mq} \quad (26)$$

$$\acute{\psi}_{rd} = \acute{\acute{L}}_{\ell r} * \acute{\imath}_{rd} + L_m * i_{md} \quad (27)$$

$$\acute{\psi}_{rq} = \acute{\acute{L}}_{\ell r} * \acute{\imath}_{rq} + L_m * i_{mq} \quad (28)$$

where i_{sd}, $\acute{\imath}_{rd}$, i_{sq}, and $\acute{\imath}_{rq}$ are stator and rotor currents in the D and Q axes respectively.

The rotor mechanical speed ω_m is calculated from the dynamic mechanical model as:

$$\frac{d\omega_m}{dt} = \frac{1}{J}\left(T_e - T_\ell - V_f * \omega_m\right) \quad (29)$$

where T_e is the electromagnetic torque of the motor, calculated as [27]:

$$T_e = \left(\frac{3}{2}\right) * P_p * L_m * (i_{sd} * \acute{\imath}_{rq} - i_{sq} * \acute{\imath}_{rd}) \quad (30)$$

where T_ℓ is the motor load torque (N.m), J is the moment of inertia ($K_g.m^2$), P_p is the magnetic pole-pair number, and V_f is the viscosity resistance factor (N.m/(rad/s)).

III. MODELING OF THE SIX-STEP VOLTAGE SOURCE INVERTER

The Matlab simulation tool was utilized for the design and analysis of the power inverter system. The switching function method can be used to represent the inverter itself. Inverter harmonics and switching losses can be calculated through simulations. The switching function method is used when the exact physical forms of the power electronic switches such as transistors and thyristors are not of concern. Using the concept of the switching function, inverters can be modeled for performance calculation. The transfer function model has several advantages in modeling VSIs. The power circuit of the inverter can be simplified into input and output variables and calculated easily, the inverter topologies can be derived easily, and the implementation of gating control pulses are simpler. Based on the theory of the transfer function of the VSI, the DC input voltage V_{dc} to the inverter and the output currents (i_a, i_b, i_c) are independent variables, while the input current I_{dc} and the output line voltages (v_{ab}, v_{bc}, v_{ca}) are dependent variables. These variables are related as [20]:

$$[v_{ab}\ , v_{bc}\ , v_{ca}\ ] = [\text{TF}]\ [V_{dc}] \quad (31)$$

$$[I_{dc}] = [\text{TF}] \quad [\ i_a\ , i_b\ , i_c\ ] \quad (32)$$

where [TF] is the transfer function of the VSI, expressed in the form of switching functions of the three-phase bridge VSI. Figure 3 shows the schematic diagram of the whole system containing the VSI fed 3-phase induction motor system. The sinusoidal 3-phase supply feeds the 3-phase uncontrolled diode bridge rectifier. A DC link with two capacitances is connected across the output diode rectifier to remove the ripple. The VSI behaves as a 3-phase voltage source to the induction motor.

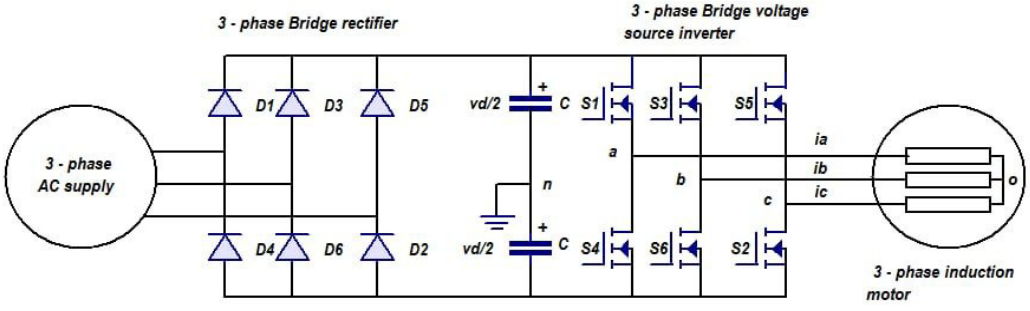

Fig. 3. Rectifier-inverter-induction motor system.

Let S_1, S_2, S_3, S_4, S_5, and S_6 be the switching functions for the three legs (a, b, c). S_1 and S_4 for pole (a), S_3 and S_6 for pole (b), and S_5 and S_2 for pole (c). The switching function is defined as 1 when the switch is ON and 0 when the switch is OFF. By applying Kirchhoff's voltage law to the closed-loop in the circuit in Figure 3, taking the conditions corresponding to the switching functions for each leg and after series manipulation, the motor (load) phase voltages become [29]:

$$v_{ao} = \frac{V_{dc}}{6}(2S_1 + S_2 - S_3 - 2S_4 - S_5 + S_6) \quad (33)$$

$$\upsilon_{bo} = \frac{V_{dc}}{6}(2S_3 + S_2 - S_2 - 2S_6 - S_5 + S_4) \quad (34)$$

$$\upsilon_{co} = \frac{V_{dc}}{6}(2S_5 + S_4 - S_4 - 2S_2 - S_3 + S_6) \quad (35)$$

The input DC (I_{dc}) to the 3-phase inverter is expressed in terms of switching functions ($S_1 \longrightarrow S_6$) and inverter output currents (i_a , i_b , i_c) as :

$$I_{dc} = (S_1 - S_4).i_a + (S_3 - S_6).i_b + (S_5 - S_2).i_c \quad (36)$$

IV. MODELING OF THE 3-PHASE BRIDGE RECTIFIER

By using the 3-phase bridge diode rectifier, the 3-phase AG input power supply (υ_a, υ_b, υ_c) is converted into the DC voltage (V_{dc}) output power supply to the inverter. The input supply voltages are given as:

$$\upsilon_a = V_m . \sin(\omega t) \quad (37)$$

$$\upsilon_b = V_m . \sin(\omega t - 2\pi/3) \quad (38)$$

$$\upsilon_c = V_m . \sin(\omega t + 2\pi/3) \quad (39)$$

where V_m is the maximum supply voltage.

The switching functions ($S_1 - S_6$) of the diode bridge rectifier have the same expression as the voltage source inverter. The input and output variables of the 3-phase diode bridge rectifier are related as:

$$\begin{bmatrix} i_a \\ i_b \\ i_c \end{bmatrix} = \begin{bmatrix} S_1 & S_4 \\ S_3 - S_6 \\ S_5 & S_2 \end{bmatrix} . [I_{dc}] \quad (40)$$

$$[V_{dc}] = [(S_1 - S_4).(S_3 - S_6).(S_5 - S_2)]. \begin{bmatrix} \upsilon_a \\ \upsilon_b \\ \upsilon_c \end{bmatrix} \quad (41)$$

The three-phase supply voltages are converted to D-Q axis components using the transformation matrix as:

$$\begin{bmatrix} V_d \\ V_q \end{bmatrix} =$$

$$\begin{bmatrix} \cos(\omega t) & \cos(\omega t + 2\pi/3) & cos(\omega t - 2\pi/3) \\ -\sin(\omega t) & -\sin(\omega t + 2\pi/3) & -sin(\omega t - 2\pi/3) \end{bmatrix} . \begin{bmatrix} \upsilon_a \\ \upsilon_b \\ \upsilon_c \end{bmatrix} \quad (42)$$

where V_d and V_q are the components of the synchronously rotating D-Q axes of the supply voltages. The output DC voltage of the bridge rectifier is expressed as:

$$V_{dc} = \frac{3.\sqrt{3}}{\pi} . \left[V_d^2 + V_q^2\right]^{\frac{1}{2}} \quad (43)$$

V. HARMONIC EQUIVALENT CIRCUIT AND PERFORMANCE CALCULATION

The proposed fundamental equivalent circuit of the induction motor is shown in Figure 1, where R_s, $X_{\ell s}$, and $R_{sss\ell}$ are the stator winding resistance, leakage reactance, and stray load loss resistance respectively, while $\acute{R}_r$, $R_{rss\ell}$, and $\acute{X}_{\ell r}$ are rotor winding resistance, stray loss resistance, and leakage reactance respectively, X_m is the magnetizing reactance, R_{ic} is the iron core loss resistance, $R_{f\omega}$ is the friction and windage (mechanical) loss resistance, and $\acute{\acute{R}}_r\,(1-s)/s$ is the motor load resistance, considering the effect of rotor stray load resistance $R_{rss\ell}$ and mechanical resistance $R_{f\omega}$ into account, as calculated by (5).

There are two types of harmonics generated in the induction motor. The first type is the space harmonic generated in the air gap as pulsating torques due to the magnetic interaction between different phases to produce the revolving magnetic field in the air gap. Space harmonics are reduced by improved design procedures and optimization [30]. These harmonics affect the motor starting and generate noise and vibration. The second type is the time-harmonics, which are generated due to the applications of variable frequency drives in modern power systems using six-step VSIs. Time harmonics increase the motor heat by increasing the motor temperature. The time-harmonic losses are generated due to the inverter switching and are impressed in the machine as additional losses. The additional time-harmonic losses are not load-dependent. For a balanced 3-phase inverter output voltage supply, only the odd harmonics should be taken into account. The third and its multiple harmonics are in the same phase and should also not be considered. Considering only the non-triple odd harmonics (5th, 7th, 11th, etc.), the Fourier series of the phase voltages are given as [27]:

$$\upsilon_a = V_{1m} . \sin(\omega_s t) + V_{5m} . \sin(5\omega_s t) + V_{7m} . \sin(7\omega_s t) + \ldots \quad (44)$$

$$\upsilon_{bo} = V_{1m} . \sin(\omega_s t - 120^{\circ}) + V_{5m} . \sin(5\omega_s t - 120^{\circ}) + V_{7m} . \sin(7\omega_s t - 120^{\circ}) + \ldots . \quad (45)$$

$$\upsilon_{co} = V_{1m} . \sin(\omega_s t + 120^{\circ}) + V_{5m} . \sin(5\omega_s t + 120^{\circ}) + V_{7m} . \sin(7\omega_s t + 120^{\circ}) + \ldots . \quad (46)$$

where V_{1m} , V_{5m} , V_{7m} are the maximum values of the fundamental, 5th, and 7th harmonic components and ω_s is the angular frequency of the supply voltage.

For each harmonic component, the motor equivalent circuit components are approximately represented by multiplying these components by a constant factor *k*, which represents the order of the harmonic. The fundamental circuit of Figure 1 is converted to a time-harmonic equivalent circuit as shown in Figure 4, taking the effect of core loss resistance R_{ic} as a voltage drop in the stator and rotor circuits. Resistances R_{ssick} and R_{rsick} are reflected series resistances of the iron core harmonic resistance R_{ick} at the stator and rotor windings [25].

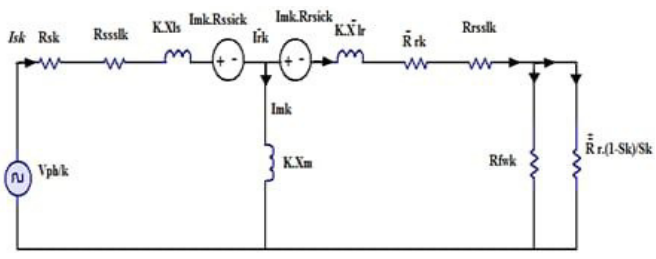

Fig. 4. Proposed equivalent circuit for time-harmonic calculation.

Equations (44)-(46) of the output inverter phase voltage indicate that the 5th harmonic voltage component has a negative phase sequence, whereas the 7th harmonic has a positive phase

sequence like the fundamental component. The magnetic flux generated in the air gap due to the 5th harmonics opposes that due to the 7th harmonics. The rotor speed is related to the fundamental frequency, and it appears practically constant concerning the harmonic field is given as [31]:

$$S_k = \frac{(k-1)+S}{k} \text{ for forwarding rotating fields} \quad (47)$$

$$S_k = \frac{(k+1)-S}{k} \text{ for backward rotating fields} \quad (48)$$

From Figure 4, if $k.X_m$ is assumed to approach infinity and $k.(X_{\ell s} + \acute{X}_{\ell r})$ is greater than R_{sk}, $R_{sss\ell}$, R_{rk}, and $R_{rss\ell}$, then the current of the *k*-th harmonic component is:

$$I_k = V_k / \left[k\,.\,(X_{\ell s} + \acute{X}_{\ell r})\right] = \frac{V_{ph}}{k^2.(X_{\ell s}+\acute{X}_{\ell r})} \quad (49)$$

The corresponding expression of the RMS harmonic ripple current I_h is obtained by the superposition principle as [18]:

$$I_h = [I_5^2 + I_7^2 + I_{11}^2 + I_{13}^2 + I_{17}^2 + \cdots]^{\frac{1}{2}} \quad (50)$$

The total stator and rotor windings copper losses and stray load losses due to the fundamental and harmonic ripple currents are obtained as:

$$\mathrm{P}_{cuss} = 3.\left(I_{phs}^2 + I_h^2\right).(R_s + R_{sss\ell}) \quad (51)$$

$$\mathrm{P}_{cuss} = 3.\left(\acute{I}_{phs}^2 + I_h^2\right).\left(\acute{R}_r + R_{rss\ell}\right) \quad (52)$$

The stray load losses are generated in the machine essentially due to hysteresis and eddy currents induced by the stator and rotor windings leakage fluxes.

If I_{phs} is the fundamental stator phase current of the motor and I_h is the total harmonic ripple of the phase current, and by applying the superposition theorem, the stator input phase current I_s when the motor is fed from the six-step VSI is obtained as :

$$I_s = \left[I_{phs}^2 + I_h^2\right]^{\frac{1}{2}} \quad (53)$$

The total input power to the motor is:

$$\mathrm{P}_{in} = 3.V_{ph}\,.I_s\,.cos\phi \quad (54)$$

The friction and windage (mechanical) power loss due to the harmonic mechanical resistance $R_{f\omega k}$ depends on the air-gap magnetizing voltage V_g and is obtained as:

$$\mathrm{P}_{f\omega k} = 3.V_g^2 / (k^2\,.\mathrm{R}_{f\omega k}) \quad (55)$$

The iron core loss of the *k*-th harmonic is obtained as:

$$\mathrm{P}_{ick} = 3.V_g^2 / R_{ick} \quad (56)$$

Then, the superposition principle is applied to find the total harmonic core losses as:

$$\mathrm{P}_{ich} = \sum_{k=5\,,7,\ldots} \mathrm{P}_{ick} \quad (57)$$

The fundamental iron core losses are obtained as:

$$\mathrm{P}_{ic} = 3.V_g^2 / R_{ic} \quad (58)$$

Then, the total iron core loss is obtained as:

$$\mathrm{P}_{ict} = \mathrm{P}_{ic} + \mathrm{P}_{ich} \quad (59)$$

The simplified formula for the *k*-th time-harmonic electromagnetic torque T_{ek} is derived by [32]:

$$\mathrm{T}_{\mathrm{ek}} = \frac{3.\acute{I}_{rk}^2\,.\acute{R}_r}{S_k\,.\omega_{sk}} = \frac{3.I_{Sk}^2\,.\acute{R}_r}{S_k\,.\omega_{sk}} \quad (60)$$

where $\omega_{sk} = k.\omega_s$ is the angular speed of the *k*-th harmonic. The *k*-th rotor harmonic current is equal to the *k*-th stator time-harmonic current because $k.X_m$ is very large. The harmonic torque is generated by the interaction between the harmonic flux of the stator and the rotor flux. The harmonic torque is smaller than the fundamental motor torque because the harmonic current and fluxes are comparable to the normal and the torque generated by the harmonic components is partially canceled by the harmonic torque that moves in the negative direction. The 5th harmonic torque opposes the 7th harmonic torque, and a similar opposition happens between the 11th and 13th harmonics [18]. The *k*-th time-harmonic mechanical output power from the motor is derived as:

$$\mathrm{P}_{mk} = \frac{3.\acute{I}_{rk}^2.\acute{R}_r\,.(1-S_k)}{S_k} \quad (61)$$

The total harmonic mechanical output power is obtained by the superposition theorem as:

$$\mathrm{P}_{mh} = \sum_{k=5\,,7,11,\ldots} \mathrm{P}_{mk} \quad (62)$$

Then, the net mechanical output power is determined as:

$$P_m = \frac{3.\acute{I}_r^2\,.\acute{R}_r\,.(1-S)}{S} - \mathrm{P}_{mh} \quad (63)$$

The efficiency of the motor fed from the six-step VSI is:

$$\eta\% = \frac{\mathrm{P}_m}{\mathrm{P}_{in}}.100 \quad (64)$$

The efficiency of the motor will drop when the machine is operated with VSI due to increasing losses and heat. The losses are dissipated as heat. The harmonic currents increase the copper and iron-core losses. This leads to a higher temperature in the stator winding, iron core, and rotor bars. The power factor $\cos(\phi)$ is defined as the ratio of the output mechanical power to the apparent input power P_a as:

$$P.F = \cos(\phi) = \frac{P_m}{P_{in}} = \frac{\mathrm{P}_m}{\sqrt{3}.V_\ell.I_\ell} \quad (65)$$

where V_ℓ and I_ℓ are the line supply voltage and the current of the motor.

The lagging power factor can be corrected by introducing capacitors. Since VSI has capacitors on the DC bus, this provides isolation of the induction motor as the load from the network, to improve the overall power factor of the system. When the VSI starts the induction motor, low frequency applies to the motor and high starting currents will be avoided. After that, the applied voltage and frequency are increased to accelerate the motor to the steady-state speed without drawing excessive current [33].

VI. RESULTS AND DISCUSSION

To examine the validity of the dynamic model of the whole system and the harmonic equivalent circuit of the motor when

fed from the six-step VSI, the motor performance is simulated in transient and steady-state operation in Matlab and the results are compared with the ones measured when the motor is fed from the sinusoidal power supply. The parameters of the fundamental equivalent circuit at 50Hz supply are given in Table I.

TABLE I. FUNDAMENTAL EQUIVALENT CIRCUIT PARAMETERS

Machine power (KW)	R_s (Ω)	$\acute{R}_r$ (Ω)	$X_{\ell s}$ (Ω)	$\acute{X}_{\ell r}$ (Ω)	X_m (Ω)	Moment of inertia (kg.m^2)
2.0	5.1	3.5	5.0	7.5	88.0	0.03

The iron-core and the mechanical loss resistances R_{ic} and $R_{f\omega}$ are varied with air-gap voltage V_g and their relations are generated by the curve-fitting technique as given in (6)-(7). The iron core resistance R_{ic} is reflected on the stator and rotor circuits to stay in the dynamic model of the 4th order, although the iron core is considered in the model. The reflecting resistances R_{ssic} and R_{rsic} are derived by (8)-(9). The stator and rotor stray load resistances are varied with stator and rotor phase resistances and are derived by (12)-(13).

A. *Results of the Dynamic Model*

Figures (5)-(8) show the starting-up motor speed, electromagnetic torque, stator phase current, and rotor phase current when the motor is fed from a 50Hz six-step VSI supply. The results show that there are harmful harmonic currents in the stator and rotor. These harmonic currents affect the motor performance by introducing pulsating torques, overheating, and noise.

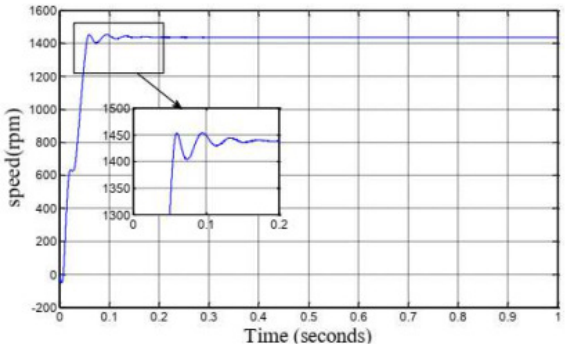

Fig. 5. Start-up motor speed with inverter supply.

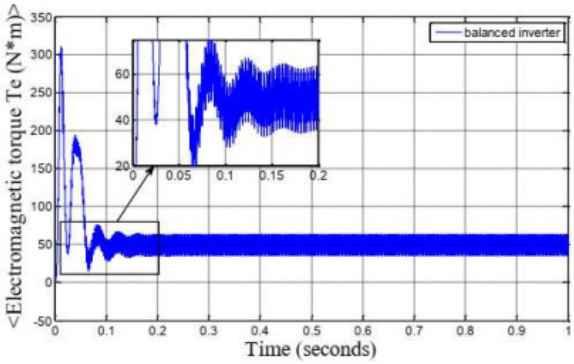

Fig. 6. Start-up motor torque with inverter supply.

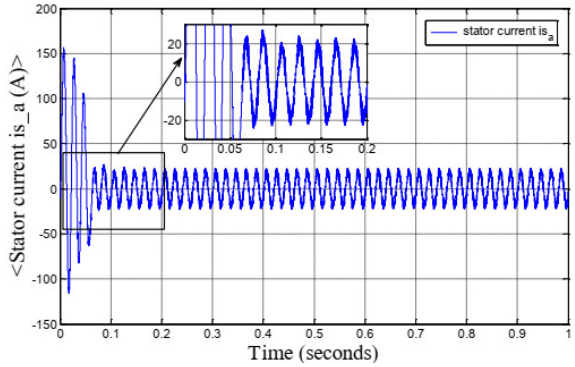

Fig. 7. Start-up motor-stator phase current with inverter supply.

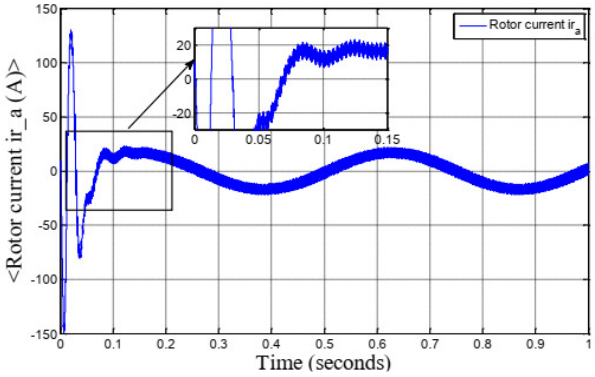

Fig. 8. Start-up motor-rotor phase current with inverter supply.

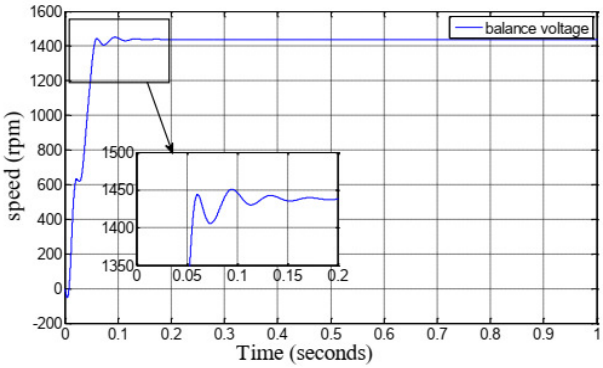

Fig. 9. Start-up motor speed with sinusoidal supply.

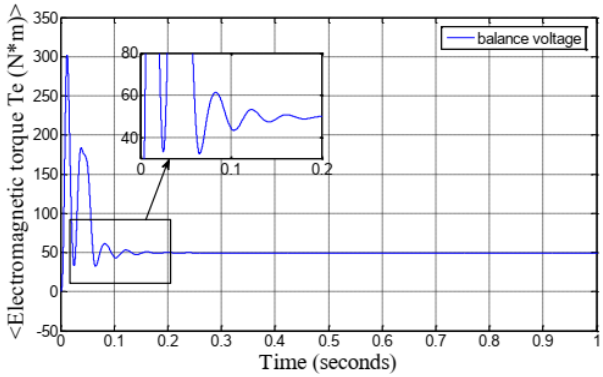

Fig. 10. Start-up motor torque with sinusoidal supply.

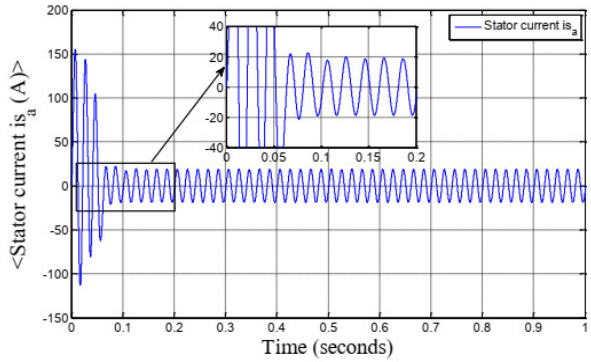

Fig. 11. Start-up motor-stator phase current with sinusoidal supply.

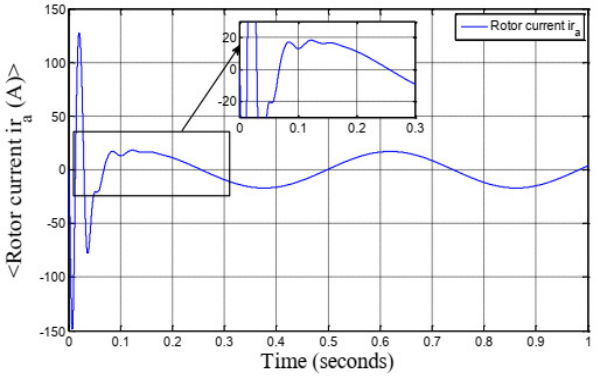

Fig. 12. Start-up motor-rotor phase current with sinusoidal supply.

Figures (9)-(12) show the starting-up motor speed, torque, stator phase current, and rotor phase current when the motor is fed from a 50Hz sinusoidal supply using the parameters of the fundamental equivalent circuit of the motor. The results show there are no harmonic currents in the stator and the rotor of the motor.

B. Results of the Harmonic Equivalent Circuit

Figure 13 compares the measured efficiency of the motor fed from the sinusoidal and VSI supplies with that produced from the simulations in Matlab. The supply current of the VSI contains high harmonics, which contribute to additional motor losses and cause the motor efficiency to decrease by 3% compared to that of the sinusoidal supply voltage at full load operation. Similarly, Figure 14 compares the measured power factor from the VSI supply with that measured from the sinusoidal supply. Due to the harmonic currents in the VSI supply, the power factor is reduced by 0.08 compared to that of the sinusoidal supply, while the power factor in Matlab simulation is higher than that of the sinusoidal supply operation by 0.05 at full load, because the harmonic currents are not considered in the fundamental equivalent circuit of the motor.

Figure 15 compares the measured total motor losses fed from the sinusoidal and VSI supplies with that of Matlab simulations predicted from the harmonic equivalent circuit and the fundamental equivalent circuit. Due to the VSI supply which contains high harmonic currents, the measured losses from the VSI fed motor are higher than those measured from the sinusoidal supply. The generated additional losses decrease the motor's efficiency. The predicted total losses from the harmonic equivalent circuit are 13% higher than that of the fundamental equivalent circuit. Figure 16 shows the detailed losses of the induction motor fed from the VSI supply predicted by the Matlab simulation of the harmonic equivalent circuit.

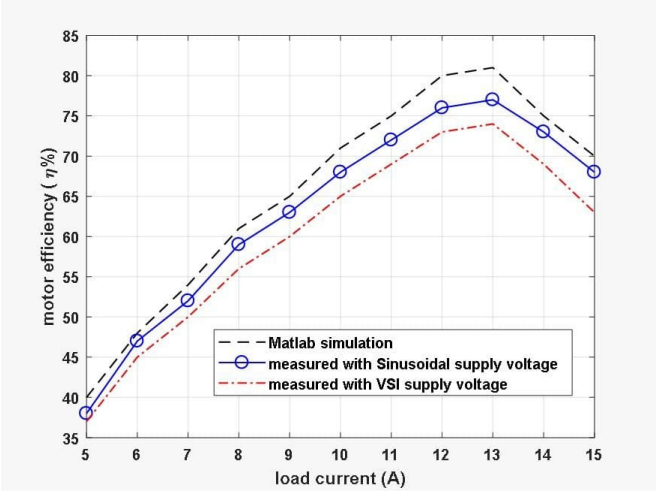

Fig. 13. Measured motor efficiency.

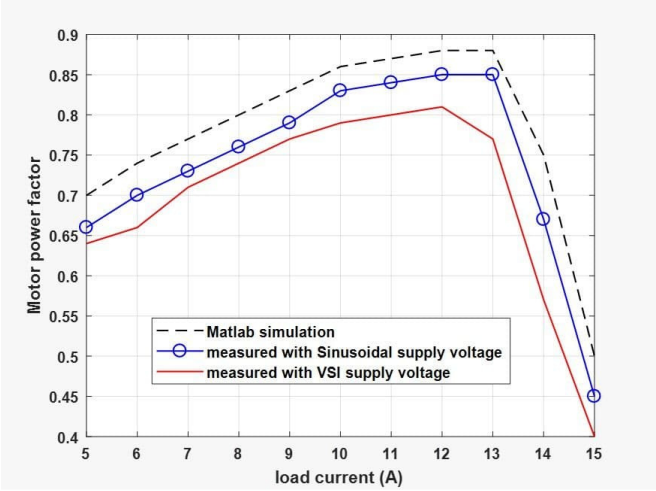

Fig. 14. Measured motor power factor.

Since the iron core loss is a function of air-gap voltage and frequency, the harmonic currents add extra losses to the iron core loss. The iron core loss reached 50% of the total losses at full load operation. Also, the presence of harmonic currents causes a rise in the losses of stator and rotor windings, according to (51)-(52). The stray load losses in the stator and rotor windings are also increased due to the harmonic currents. The friction and windage losses are assumed to be fixed and not affected by the harmonic currents.

VII. CONCLUSION

The recent developments in power electronics and semi-conductor material technologies improved power electronic AC

drive systems. Different circuit topologies of inverters, such as the six-step VSI have been used. In the six-step VSI fed induction motor, low order time harmonics (5^{th}, 7^{th}, 11^{th}) that lead to additional motor losses are generated. These additional losses are not load-depended and are estimated as the difference between the no-load losses with VSI and the sinusoidal supply. The increase of total losses in the VSI supply by nearly 20% is caused by the time-harmonic currents generated by the VSI and the conduction and switching losses of the inverter. As expected, the motor efficiency with PWM-VSI supply is lower than that with the sinusoidal supply by about 3%.

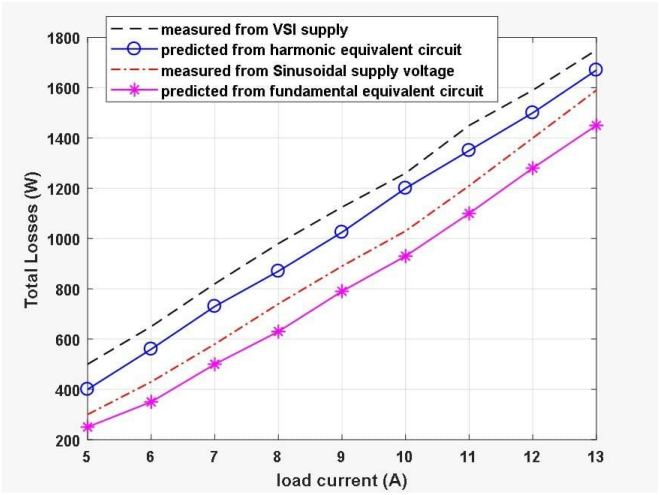

Fig. 15. Measured total motor losses.

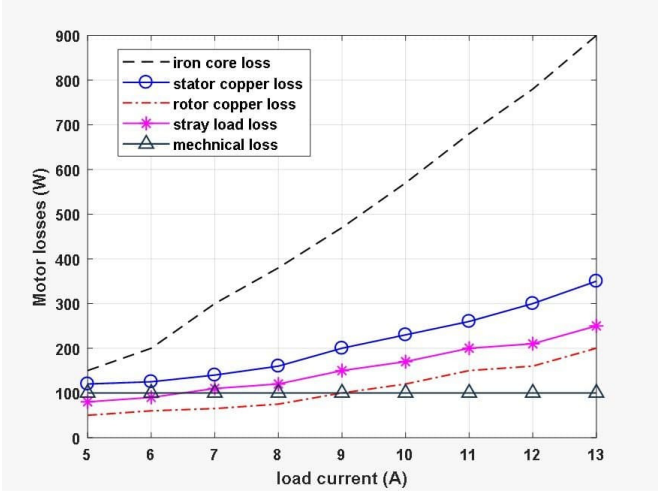

Fig. 16. Details of motor losses with VSI supply.

The stray load loss is increased by 30% with the VSI supply in comparison with the sinusoidal supply. The core losses at rated power are increased by 50% with the VSI supply, because these losses depend on the air-gap voltage and supply frequency. When the motor is operated with a VSI supply instead of a sinusoidal supply, the motor power factor is reduced by 0.08 and the stator and rotor copper losses are increased by 30% due to the harmonic current and the skin effect. The additional losses generated with the VSI supply lead to a higher temperature in the stator and rotor windings. The harmonic currents lead to extra reactive currents resulting to a decrease of the motor power factor. When the motor operates by a VSI supply, it applies low frequency and voltage to the motor in order to avoid the high inrush current. The motor supply voltage must be kept in the same proportion with the supply frequency for all motor speeds to maintain the rated torque constant and to avoid magnetic saturation. By good design of the motor structure and the output passive filter, and increasing the inverter switching frequency, the harmonics can be mitigated.

REFERENCES

[1] E. A. Klingshirn and H. E. Jordan, "Polyphase Induction Motor Performance and Losses on Nonsinusoidal Voltage Sources," *IEEE Transactions on Power Apparatus and Systems*, vol. PAS-87, no. 3, pp. 624–631, Mar. 1968, https://doi.org/10.1109/TPAS.1968.292172.

[2] B. J. Chalmers and B. R. Sarkar, "Induction-motor losses due to nonsinusoidal supply waveforms," *Proceedings of the Institution of Electrical Engineers*, vol. 115, no. 12, pp. 1777–1782, Dec. 1968, https://doi.org/10.1049/piee.1968.0311.

[3] H. Raphael, "Additional Losses in Pwm Inverter-Fed Squirrel Cage Motors," presented at the Conf Rec IAS 12th Annual Meeting, Los Angeles, CA, USA, Oct. 1977.

[4] F. G. G. D. Buck, "Losses and Parasitic Torques in Electric Motors Subjected to PWM Waveforms," *IEEE Transactions on Industry Applications*, vol. IA-15, no. 1, pp. 47–53, Jan. 1979, https://doi.org/10.1109/TIA.1979.4503611.

[5] G. C. D. Sousa, B. K. Bose, J. Cleland, R. J. Spiegel, and P. J. Chappell, "Loss modeling of converter induction machine system for variable speed drive," in *and Automation Proceedings of the 1992 International Conference on Industrial Electronics, Control, Instrumentation*, Aug. 1992, pp. 114–120 vol.1, https://doi.org/10.1109/IECON.1992.254595.

[6] K. Bradley, W. Cao, J. Clare, and P. Wheeler, "Predicting Inverter-Induced Harmonic Loss by Improved Harmonic Injection," *IEEE Transactions on Power Electronics*, vol. 23, no. 5, pp. 2619–2624, Sep. 2008, https://doi.org/10.1109/TPEL.2008.2002329.

[7] A. Boglietti, A. Cavagnino, A. M. Knight, and Y. Zhan, "Factors Affecting Losses in Induction Motors with Non-Sinusoidal Supply," in *2007 IEEE Industry Applications Annual Meeting*, Sep. 2007, pp. 1193–1199, https://doi.org/10.1109/07IAS.2007.187.

[8] W. Cao, K. J. Bradley, H. Zhang, and I. French, "Experimental Uncertainty in Estimation of the Losses and Efficiency of Induction Motors," in *Conference Record of the 2006 IEEE Industry Applications Conference Forty-First IAS Annual Meeting*, Jul. 2006, vol. 1, pp. 441–447, https://doi.org/10.1109/IAS.2006.256558.

[9] A. Vamvakari, A. Kandianis, A. Kladas, and S. Manias, "High fidelity equivalent circuit representation of induction motor determined by finite elements for electrical vehicle drive applications," *IEEE Transactions on Magnetics*, vol. 35, no. 3, pp. 1857–1860, May 1999, https://doi.org/10.1109/20.767395.

[10] Z. C. Papazacharopoulos, A. G. Kladas, and S. N. Manias, "Investigation of the switching frequency harmonics impact on PWM induction motor drive efficiency," in *2001 IEEE 32nd Annual Power Electronics Specialists Conference (IEEE Cat. No.01CH37230)*, Jun. 2001, vol. 2, pp. 1203–1208, https://doi.org/10.1109/PESC.2001.954283.

[11] Z. K. Papazacharopoulos, K. V. Tatis, A. G. Kladas, and S. N. Manias, "Dynamic model for harmonic induction motor analysis determined by finite elements," *IEEE Transactions on Energy Conversion*, vol. 19, no. 1, pp. 102–108, Mar. 2004, https://doi.org/10.1109/TEC.2003.821825.

[12] T. C. Green, C. A. Hernández-Arámburo, and A. C. Smith, "Losses in grid and inverter supplied induction machine drives," *IEE Proceedings - Electric Power Applications*, vol. 150, no. 6, pp. 712–724, Nov. 2003, https://doi.org/10.1049/ip-epa:20030848.

[13] J. M. D. Murphy and M. G. Egan, "A comparison of PWM strategies for inverter-fed induction motors," *IEEE Transactions on Industry Applications*, vol. 19, no. 3, pp. 363–369, May 1983, https://doi.org/10.1109/TIA.1983.4504210.

[14] F. C. Zach and H. Ertl, "Efficiency optimal control for AC drives with PWM inverters," *IEEE Transactions on Industry Applications*, vol. 21, no. 4, pp. 987–1000, Jul. 1985, https://doi.org/10.1109/TIA.1985.349569.

[15] S. Chen and S.-N. Yeh, "Optimal efficiency analysis of induction motors fed by variable-voltage and variable-frequency source," *IEEE Transactions on Energy Conversion*, vol. 7, no. 3, pp. 537–543, Sep. 1992, https://doi.org/10.1109/60.148576.

[16] T. Kataoka, Y. Kandatsu, and T. Akasaka, "Measurement of equivalent circuit parameters of inverter fed induction motors," *IEEE Transactions on Magnetics*, vol. 23, no. 5, pp. 3014–3016, Sep. 1987, https://doi.org/10.1109/TMAG.1987.1065440.

[17] M. Satheesh Kumar, P. Ramesh Babu, and S. Ramprasath, "Four Quadrant Operation of Direct Torque Control-SVPWM based three phase Induction Motor Drive in MATLAB/SIMULINK environment," in *2012 IEEE International Conference on Advanced Communication Control and Computing Technologies (ICACCCT)*, Dec. 2012, pp. 397–402, https://doi.org/10.1109/ICACCCT.2012.6320810.

[18] R .Prejbeanu, "Methods to Reduce the Harmonics Generated in the Asynchronous Motor Fed by Power Converter," *Annals of The University of Craiova, Series: Automation, Computers, Electronics and Mechatronics*, vol. 11 (38), no. 1, pp. 45–50, 2014.

[19] R. S. Kanchan and R. R. Moghaddam, "On accuracy of loss models including VSD induced additional harmonic losses for online energy efficient control of induction motor," in *2017 IEEE 12th International Conference on Power Electronics and Drive Systems (PEDS)*, Honolulu, HI, USA, Sep. 2017, pp. 1178-1183, https://doi.org/10.1109/PEDS.2017.8289110.

[20] D. Uma and K. Vijayarekha, "Modeling and simulation of VSI fed induction motor drive in Matlab Simulink", *International Journal of Electrical and Computer Engineering*, vol. 7, no. 2, pp. 584-595, Apr. 2017, http://doi.org/10.11591/ijece.v7i2.pp584-595.

[21] S. Firdoush, S. Kriti, A. Raj, and S. K. Singh, "Reduction of Harmonics in Output Voltage of Inverter," *International Journal of Engineering Research & Technology*, vol. 4, no. 2, Apr. 2018, https://doi.org/10.17577/IJERTCONV4IS02021.

[22] U. B. Tayab and M. A. A. Humayun, "Modeling and Analysis of a Cascaded Battery-Boost Multilevel Inverter Using Different Switching Angle Arrangement Techniques," *Engineering, Technology & Applied Science Research*, vol. 7, no. 2, pp. 1450–1454, Apr. 2017, https://doi.org/10.48084/etasr.1094.

[23] V. T. Ha, P. T. Giang, and V. H. Phuong, "T-Type Multi-Inverter Application for Traction Motor Control," *Engineering, Technology & Applied Science Research*, vol. 12, no. 2, pp. 8321–8327, Apr. 2022, https://doi.org/10.48084/etasr.4776.

[24] D. A. Tuan, P. Vu, and N. V. Lien, "Design and Control of a Three-Phase T-Type Inverter using Reverse-Blocking IGBTs," *Engineering, Technology & Applied Science Research*, vol. 11, no. 1, pp. 6614–6619, Feb. 2021, https://doi.org/10.48084/etasr.3954.

[25] B. A. Nasir, "An Accurate Iron Core Loss Model in Equivalent Circuit of Induction Machines," *Journal of Energy*, vol. 2020, Feb. 2020, Art. no. 7613737, https://doi.org/https://doi.org/10.1155/2020/7613737.

[26] B. A. Nasir, "Modeling of self-excited induction generator in synchronously rotating frame," *International Journal of Electrical & Computer Sciences*, vol. 20, no. 1, pp. 1–6, May 2020.

[27] B. A. Nasir and R. W. Daoud, "Modeling of wind turbine-self excited induction generator system with pitch angle and excitation capacitance control," *AIP Conference Proceedings*, vol. 2307, no. 1, Dec. 2020, Art. no. 020022¸ https://doi.org/10.1063/5.0032904.

[28] O. M. Al-Barbarawi, "Improving Performance of the Braking Process, and Analysis Torque-Speed Characteristics of the Induction Motor," *Engineering, Technology & Applied Science Research*, vol. 8, no. 6, pp. 3585–3591, Dec. 2018, https://doi.org/10.48084/etasr.2325.

[29] N. Htin Win and T. Naing, "Develop a Switching Function Model and Experimental Validation of Three-Phase Step- Wave Inverter Between 120˚-180˚ conduction," in *2018 Joint International Conference on Science, Technology and Innovation, Mandalay by IEEE*, Mandalay, Myanmar, Jul. 2019.

[30] B. A. Nasir, "Design of Squirrel-Cage Self-Excited 3-phase Induction Generator," *International Journal of Engineering and Advanced Technology*, vol. 11, no. 1, pp. 181–188, Jul. 2021, https://doi.org/10.35940/ijeat.A3198.1011121.

[31] B. K. Bose, "The Effect of Harmonics," in *Modern Power Electronics and AC Drives*, Upper Saddle River, N.J, USA: Prentice Hall PTR, 2002, pp. 49–55.

[32] E. O. Anyang, "The impact of variable speed drives on energy efficient induction motors," M.S. thesis, University of Cape Town, Cape Town, South Africa, 2011.

[33] N. H. Mugheri and M. U. Keerio, "An Optimal Fuzzy Logic-based PI Controller for the Speed Control of an Induction Motor using the V/F Method," *Engineering, Technology & Applied Science Research*, vol. 11, no. 4, pp. 7399–7404, Aug. 2021, https://doi.org/10.48084/etasr.4255.